First-Row Transition Metal Complexes of the Hexadentate Macrocycle 1,4,7-Tris(5-*tert*-butyl-2-hydroxybenzyl)-1,4,7-triazacyclononane (LH_3). Crystal Structures of $[LTi^{IV}]BPh_4$, $[LCr^{III}]$, $[LFe^{III}]$, and $[(LH)_2Fe^{III}_2](ClO_4)_2 \cdot 2H_2O$

Ulf Auerbach,[1a] Thomas Weyhermüller,[1a] Karl Wieghardt,*[,1a] Bernhard Nuber,[1b] Eckhard Bill,[1c] Christian Butzlaff,[1c] and Alfred X. Trautwein[1c]

Lehrstuhl für Anorganische Chemie I, Ruhr-Universität, D-4630 Bochum, Germany, Anorganisch-Chemisches Institut der Universität, D-6900 Heidelberg, Germany, and Institut für Physik, Medizinische Universität, D-2400 Lübeck, Germany

Received April 23, 1992

The new hexadentate macrocycle containing three phenolate pendant arms has been prepared from 1,4,7-triazacyclononane and 3 equiv of 2-bromomethyl-4-*tert*-butylphenyl acetate: Tripotassium 1,4,7-tris(5-*tert*-butyl-2-hydroxybenzyl)-1,4,7-triazacyclononanate (K_3L; $C_{39}H_{54}N_3O_3K_3$). The reaction of trivalent first-row transition metals with the trianion affords monomeric pseudooctahedral complexes, of which the following have been characterized: LV^{III} (**2**); LCr^{III} (**5**); LMn^{III} (**6**); LFe^{III} (**8**); LCo^{III} (**9**). Monocationic complexes containing a tetravalent metal ion have also been prepared: $[LTi^{IV}]PF_6$; $[LV^{IV}](ClO_4)$ (**3**); $[LMn^{IV}]BPh_4$ (**7**). $[LV^{V}](ClO_4)_2$ (**4**) has been synthesized by oxidation of **2** or by reaction of NH_4VO_3 and K_3L in acidic CH_3CN solution. In acidic methanolic solutions of **5**, **8**, and **9** dimeric species were obtained as crystalline solids: $[(LH)_2M^{III}_2](ClO_4)_2 \cdot 2H_2O$ (M = Cr^{III} (**10**), Fe^{III} (**11**), Co^{III} (**12**)). The crystal structures of $[LTi^{IV}]BPh_4$, **5**, **8**, and **11** have been determined by X-ray crystallography: $[LTi]BPh_4$, orthorhombic, space group $P2_12_12_1$, a = 10.856(6) Å, b = 19.33(2) Å, c = 26.49(2) Å, Z = 4; **5**, trigonal, space group $R3$, a = 23.547(3) Å, c = 6.521(1) Å, Z = 3; **8**, trigonal, space group $R3$, a = 23.64(2) Å, c = 6.599(7) Å, Z = 3; **11**, monoclinic, space group $P2_1/n$, a = 16.48(1) Å, b = 13.78(1) Å, c = 17.84(1) Å, β = 93.72(6)°; Z = 2. Electronic spectral data, magnetic properties, and the electrochemistry of the new complexes are reported. The d_π–p_π bonding of the phenolate–metal M–O bonds is analyzed as a function of the d^n electronic configuration of the respective metal ion.

Introduction

Hexadentate ligands containing a 1,4,7-triazacyclononane backbone and three N-bonded phenolate pendant arms (Scheme I) have recently attracted a great deal of interest.[2,3] Complexes of these ligands with ^{67,68}Ga and ^{111}In radioisotopes are of interest as imaging agents.[4-6] Martell and Motekaitis have reported that two ligands of this type, namely 1,4,7-tris(3-hydroxy-6-methyl-2-methylpyridyl)-1,4,7-triazacyclononane[7] and 1,4,7-tris(3,5-dimethyl-2-hydroxybenzyl)-1,4,7-triazacyclononane,[8] can bind iron(III) as strongly or even more efficiently than the natural siderophore enterobactin. Ligands of this type are considered to be promising drugs for the treatment of iron overload (thalassaemia).[9]

We had prepared the analogous ligands 1,4,7-tris(2-hydroxybenzyl)-1,4,7-triazacyclononane and 1,4,7-tris(3-*tert*-butyl-2-hydroxybenzyl)-1,4,7-triazacyclononane and reported their coordination chemistry with first-row transition metals including iron(III).[3] It was found that the neutral complexes with trivalent metal ions are quite insoluble in most common solvents and are therefore not readily characterized in solution. Here we report the synthesis (Scheme II) and coordination chemistry of 1,4,7-tris(5-*tert*-butyl-2-hydroxybenzyl)-1,4,7-triazacyclononane (LH_3). Some results of this work have been communicated previously.[10] As we will show, the stability of LM, $[LM]^+$, and $[LM]^{2+}$ species is very large and their solubility in polar organic solvents is in general quite good. We have obtained single crystals for X-ray structure determinations. It has been possible to study the degree of d_π–p_π bonding in the M–$O_{phenolate}$ bonds as a function of the d^n electronic configuration of the central metal ion.

Scheme I

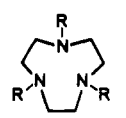

R:		Ref.
	2-Hydroxybenzyl	[3]
	3,5-Dimethyl-2-hydroxybenzyl	[2]
	3-tert.-Butyl-2-hydroxybenzyl	[3]
	3-Hydroxy-6-methyl-2-pyridylmethyl	[7]
	5-tert.-Butyl-2-hydroxybenzyl	this work

Experimental Section

1,4,7-Triazacyclononane was prepared according to published procedures.[11] 2-Methyl-4-*tert*-butylphenol was purchased from Aldrich and used as received.

Synthesis of the Ligand Tripotassium 1,4,7-Tris(5-*tert*-butyl-2-hydroxybenzyl)-1,4,7-triazacyclononanate (K_3L). A solution of 2-methyl-4-*tert*-butyl-phenol (16.4 g; 0.1 mol) in acetic anhydride (20.4 g; 0.2 mol) and a few drops of concentrated H_2SO_4 was stirred at room temperature for 15 h. Acetic acid and acetic anhydride were removed in vacuo, and the resulting red oil was distilled (yield of 19.5 g of 2-methyl-4-*tert*-butylphenyl acetate (95%)) and dissolved in CCl_4 (100 mL). After addition of *N*-bromosuccinimide (17.8 g; 0.1 mol) and azobisisobutyronitrile (0.10 g) the solution was gently heated until the very exothermic

(1) (a) Ruhr-Universität Bochum. (b) Universität Heidelberg. (c) Medizinische Universität Lübeck.
(2) Moore, D. A.; Fanwick, P. E.; Welch, M. J. *Inorg. Chem.* **1989**, *28*, 1504.
(3) Auerbach, U.; Eckert, U.; Wieghardt, K.; Nuber, B.; Weiss, J. *Inorg. Chem.* **1990**, *29*, 938.
(4) Moerlein, S. M.; Welch, M. J.; Raymond, K. N.; Weitl, J. *J. Nucl. Med.* **1981**, *22*, 710.
(5) Mathias, C. J.; Sun, Y.; Welch, M. J.; Green, M. A.; Thomas, J. A.; Wade, K. R.; Martell, A. E. *Nucl. Med. Biol.* **1988**, *15*, 69.
(6) Mathias, C. J.; Sun, Y.; Welch, M. J.; Green, M. A.; Thomas, J. A.; Wade, K. R.; Martell, A. E. *J. Labelled Comp. Radiopharm.* **1986**, *23*, 1221.
(7) Martell, A. E.; Motekaitis, R. J.; Welch, M. J. *J. Chem. Soc., Chem. Commun.* **1990**, 1748.
(8) Clarke, E. T.; Martell, A. E. *Inorg. Chim. Acta* **1991**, *186*, 103.
(9) Bradley, D. *New Sci.* **1991**, *35*.
(10) Auerbach, U.; Della Vedova, B. S. P. C.; Wieghardt, K.; Nuber, B.; Weiss, J. *J. Chem. Soc., Chem. Commun.* **1990**, 1004.
(11) (a) Wieghardt, K.; Schmidt, W.; Nuber, B.; Weiss, J. *Chem. Ber.* **1979**, *112*, 2220. (b) Atkins, T. J.; Richman, J. E.; Oettle, W. F. *Org. Synth.* **1978**, *58*, 86.

0020-1669/93/1332-0508$04.00/0

Scheme II

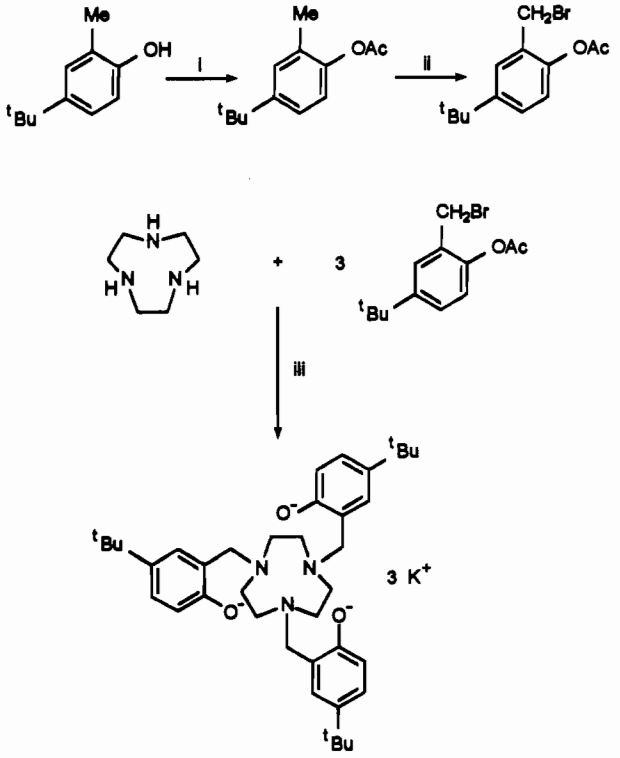

bromination reaction started. The solution was then stirred for 2 h at ambient temperature. After filtration and removal of the solvent in vacuo the product was distilled. The fraction 125–135 °C at 0.03 mmHg was collected. Yield of 2-bromomethyl-4-*tert*-butylphenyl acetate: 20–27 g (70–95%).

To a solution of 1,4,7-triazacyclononane (12.9 g; 0.10 mol) in toluene (50 mL) was added dropwise with stirring at 20 °C within 5 min a solution of 2-bromomethyl-4-*tert*-butylphenyl acetate (85.6 g; 0.30 mol) in toluene (30 mL). A viscous mud-colored oil formed which stuck to the surface of the reaction vessel. After the mixture was stirred for 30 min, solid, powdered KOH (33.7 g; 0.60 mol) was carefully added. The reaction mixture was gently heated to 60–70 °C until the very exothermic neutralization reaction started. (*Caution*: The reaction can be very violent.) The temperature was maintained between 40 and 60 °C by efficient cooling until the reaction subsided. Toluene (200 mL) was added to the reaction mixture, which was stirred at room temperature for 8 h and filtered. The solid residue was washed thoroughly three to four times with water (100 mL). The residual gray-white solid is the desired product K_3L, which was used for the synthesis of complexes without further purification. Further product was obtained from the above filtrate by removing the solvent in vacuo whereupon a red, very viscous oil or nearly solid material was obtained. This material was dissolved in ethanol (70–100 mL) at ambient temperature (2–3 h). The solution was stirred for 12 h, during which time a colorless precipitate of K_3L formed which was collected by filtration. K_3L is only sparingly soluble in all common organic solvents and water. Yield: 35–45 g (48–62%). ^1H NMR (80 MHz; $CDCl_3$): δ 1.35 (s, 27 H; $C(CH_3)_3$), 2.85 (s, 12 H; $N(CH_2)_2N$), 3.75 (s, 6 H; $N(CH_2)$–Ar), 6.7–7.2 (m, 9 H; aromatic protons). IR (KBr disk): ν(C–O) 1253 cm^{-1}. UV–vis (CH_2Cl_2) 285 nm ($\epsilon = 7.9 \times 10^3$ L mol^{-1} cm^{-1}). Anal. Calcd for $C_{39}H_{54}N_3O_3K_3$: C, 64.2; H, 7.5; N, 5.8. Found: C, 64.2; H, 7.3; N, 5.6.

Synthesis of Complexes. [LTi^{IV}](PF$_6$) (1). A mixture of $TiCl_3$ (0.15 g; 1.0 mmol) in acetonitrile (50 mL) was heated under an argon blanketing atmosphere until a clear blue solution was obtained. Addition of K_3L (0.73 g; 1.0 mmol) and triethylamine (2 mL) initiated the precipitation of a green solid within 5 min. Upon exposure of this suspension to air a clear yellow solution formed within seconds. To the filtered solution was added $NaPF_6$ (0.10 g). Yellow crystals precipitated from this solution within 2–3 d at room temperature, which were collected by filtration. Yield: 0.57 g (86%). Yellow crystals of [LTi]BPh_4 suitable for X-ray crystallography were grown from an acetonitrile solution of [LTi](PF_6) to which an equimolar amount of $NaBPh_4$ had been added. Anal. Calcd for $C_{39}H_{54}F_6N_3O_3PTi$: C, 58.1; H, 6.8; N, 5.2. Found: C, 57.6; H, 6.8; N, 5.1.

[LV^{III}] (2). A mixture of VCl_3 (0.157 g; 1.0 mmol) in acetonitrile (50 mL) was heated to reflux under an argon atmosphere until a clear green solution was obtained. Addition of K_3L (0.73 g; 1.0 mmol) and $N(Et)_3$ (2 mL) to the hot solution initiated the precipitation of a green solid. Addition of degassed water (50 mL) caused the precipitation of LV in essentially quantitative yield (0.64 g; 96%). The solid complex is stable in air and reasonably soluble in polar organic solvents. Anal. Calcd for $C_{39}H_{54}N_3O_3V$: C, 70.6; H, 8.2; N, 6.3. Found: C, 69.8; H, 8.4; N, 6.2.

[LV^{IV}](ClO$_4$) (3). To a suspension of [LV] (0.66 g; 1.0 mmol) in methanol (50 mL) was added concentrated $HClO_4$ (5 mL) at 20 °C. *Caution*: This is a potentially hazardous procedure (explosive)! Within 1 h a clear solution formed in the presence of air. From this solution violet microcrystals formed within 4 d. Addition of excess $NaBPh_4$ initiates the crystallization of large cubic crystals of [LV]BPh_4. Anal. Calcd for $C_{39}H_{54}N_3O_7ClV$: C, 61.4; H, 7.1; N, 5.5. Found: C, 61.2; H, 7.0; N, 5.3.

[LV^{V}](ClO$_4$)$_2$ (4). Method A. *Caution*: This procedure is potentially hazardous due to the possible formation of perchloric acid methyl ester! To a solution of **3** (0.76 g; 1.0 mmol) in methanol (50 mL) was added concentrated $HClO_4$ (10 mL). After the mixture was stirred for 5 h at 20 °C in the presence of air another portion of concentrated $HClO_4$ (10 mL) was added. A color change from violet to deep blue was observed. Deep blue-black microcrystals precipitated from this solution over night. Yield: 0.72 g (83%).

Method B. A solution of K_3L (0.73 g; 1.0 mmol) and NH_4VO_3 (0.12 g; 1.0 mmol) in CH_3CN (50 mL) was heated to reflux for 1 h. To the cooled (50 °C) solution was added concentrated $HClO_4$ (5 mL) whereupon a rapid color change to deep blue was observed. The filtered solution (removal of $KClO_4$) was allowed to stand in an open vessel for 2–3 d. A microcrystalline blue precipitate formed. Yield: 0.38 g (44%). Anal. Calcd for $C_{39}H_{54}Cl_2N_3O_{11}V$: C, 54.4; H, 6.3; N, 4.9. Found: C, 54.6; H, 6.5; H, 4.9.

[LCr^{III}] (5). A suspension of $CrCl_3 \cdot 6H_2O$ (0.26 g; 1.0 mmol), K_3L (0.73 g; 1.0 mmol), and a small amount of activated, granulated zinc in acetonitrile (50 mL) was heated to reflux, and $N(Et)_3$ (2 mL) was added. The mixture was heated to reflux for 12 h, during which time a pink precipitate formed which was collected by filtration and recrystallized from methanol to which a few drops of concentrated $HClO_4$ were added. Yield: 0.64 g (96%). Anal. Calcd for $C_{39}H_{54}N_3O_3Cr$: C, 70.5; H, 8.2; N, 6.3. Found: C, 70.2; H, 8.4; N, 6.2.

[LMn^{III}] (6). A solution of K_3L (0.73 g; 1.0 mmol) and manganese(III) acetate in methanol (50 mL) was stirred at room temperature for 1 h. From the green solution a green solid precipitated. Addition of water resulted in a nearly quantitative precipitation of [LMn^{III}], which was recrystallized from dimethylformamide. Yield: 0.64 g (96%). Anal. Calcd for $C_{39}H_{54}MnN_3O_3$: C, 70.1; H, 8.2; N, 6.3. Found: C, 70.3; H, 7.9; N, 6.1.

[LMn^{IV}]BPh$_4$ (7). To a suspension of **6** (0.67 g; 1.0 mmol) in methanol (50 mL) was added concentrated $HClO_4$ (5.0 mL). *Caution*: This procedure is potentially hazardous! After the mixture was stirred for 1 h in the presence of air, a deep blue clear solution was obtained from which blue crystals of [LMn](ClO_4) precipitated within a few hours. The tetraphenylborate salt was obtained from a methanol solution of this material by addition of an excess Na[BPh_4]. Blue crystals of [LMn]-BPh_4 were recrystallized from an acetonitrile solution. Yield: 0.69 g (70%). Anal. Calcd for $C_{63}H_{74}BMnN_3O_3$: C, 76.7; H, 7.6; N, 4.3. Found: C, 76.3; H, 7.9; N, 4.1.

[LFe^{III}] (8). A solution of $Fe(ClO_4)_3 \cdot 6H_2O$ (0.46 g; 1.0 mmol) and K_3L (0.73 g; 1.0 mmol) in methanol (50 mL) was stirred at room temperature for 30 min. After addition of $N(Et)_3$ (10 mL) the stirring was continued for 4 h, during which time a color change from blue to red was observed. Addition of water (50 mL) initiated the precipitation of a red solid, which was recrystallized from dimethoxyethane. Yield: 0.65 g (97%). Anal. Calcd for $C_{39}H_{54}FeN_3O_3$: C, 70.1; H, 8.1; N, 6.3. Found: C, 69.8; H, 8.3; N, 6.1.

[LCo^{III}] (9). To a solution of K_3L (0.73 g; 1.0 mmol) and triethylamine (10 mL) in acetone (50 mL) was added $Co(ClO_4)_2 \cdot 6H_2O$ (0.37 g; 1.0 mmol). The solution was stirred at room temperature in the presence of air for 12 h. A green solution formed from which a green solid precipitated which is nearly insoluble in all common organic solvents. Yield: 0.65 g (97%). Anal. Calcd for $C_{39}H_{54}CoN_3O_3$: C, 69.7; H, 8.1; N, 6.3. Found: C, 69.3; H, 8.0; N, 6.2.

[(LH)$_2$Cr$^{III}_2$](ClO$_4$)$_2 \cdot$2H$_2$O (10). To a suspension of **5** (0.66 g; 1.0 mmol) in methanol (50 mL) was added concentrated $HClO_4$ (5 mL). Within a few minutes of stirring at room temperature a clear violet solution was obtained from which violet crystals precipitated within 2–3 d. In

Table I. Crystallographic Data for [LTi]BPh_4 (**1**), [LCr] (**5**), [LFe] (**8**), and $[Fe_2(LH)_2](ClO_4)_2 \cdot 2H_2O$ (**11**)

	1	**5**	**8**	**11**
formula	$C_{63}H_{74}BN_3O_3Ti$	$C_{39}H_{54}CrN_3O_3$	$C_{39}H_{54}FeN_3O_3$	$C_{78}H_{114}Cl_2Fe_2N_6O_{16}$
fw	979.99	664.9	668.7	1574.4
a, Å	10.856(6)	23.547(3)	23.64(2)	16.48(1)
b, Å	19.33(2)			13.78(1)
c, Å	26.49(2)	6.521(1)	6.599(7)	17.84(1)
β, deg				93.72(6)
V, Å^3	5558.8(9)	3131.2(7)	3193.8(8)	4042.8(13)
Z	4	3	3	2
space group	$P2_12_12_1$ (No. 19)	$R3$ (No. 146)	$R3$ (No. 146)	$P2_1/n$ (No. 14)
T, °C	22(1)	22(1)	22(1)	22(1)
λ, Å	0.710 73	0.710 73	0.710 73	0.710 73
ρ_{calc}, g cm^{-3}	1.17	1.057	1.04	1.29
μ, mm^{-1}	0.20	0.298	0.38	0.49
transm coeff: max; min	1.0–0.95	0.535–0.516	1.0–0.97	0.867–0.745
R^a	0.066	0.066	0.066	0.086

^{a} $R = \sum||F_o| - |F_c||/\sum|F_o|$.

contrast to **5**, **10** is readily soluble in polar solvents. Yield: 0.47 g (60%). Anal. Calcd for $C_{78}H_{114}Cl_2Cr_2N_6O_{16}$: C, 59.8; H, 7.3; N, 5.4; Cl, 4.5. Found: C, 59.9; H, 7.1; N, 5.5; Cl, 4.3.

$[(LH)_2Fe^{III}_2](ClO_4)_2 \cdot 2H_2O$ (11). This blue complex was prepared as described for **10** by using **8** as starting material. Yield: 0.45 g (57%). Anal. Calcd for $C_{78}H_{114}Cl_2Fe_2N_6O_{16}$: C, 59.5; H, 7.3; N, 5.3; Cl, 4.5. Found: C, 59.4; H, 7.1; N, 5.5; Cl, 4.5.

$[(LH)_2Co^{III}_2](ClO_4)_2 \cdot 2H_2O$ (12). This green complex was prepared as described for **10** and **11** by using **9** as starting material. Yield: 0.55 g (70%). Anal. Calcd for $C_{78}H_{114}Cl_2Co_2N_6O_{16}$: C, 59.3; H, 7.3; N, 5.3. Found: C, 58.9; H, 7.1; N, 5.2.

Physical Measurements. Infrared spectra were recorded in the range 4000–400 cm^{-1} as KBr disks on a Perkin–Elmer Model 1720 X FT-IR spectrometer. Electronic absorption spectra were measured in the range 200–1500 nm on a Perkin-Elmer Lambda 9 spectrophotometer. The 400-MHz ^{1}H NMR spectra were recorded on a Bruker AM 400 FT spectrometer at a magnetic field of 400.13 MHz with the solvent as internal standard; the ^{13}C NMR spectra at a field of 100.6 MHz. ESR spectra were recorded on a Bruker ER 200 D X-band spectrometer, equipped with a standard TE 102 resonator (ER 4102, Bruker) and a helium-flow cryostat (ESR 910, Oxford instruments). The magnetic susceptibilities of powdered samples of complexes were measured either in the temperature range 80–295 K by using the Faraday method or in the range 2–295 K on a SQUID magnetometer (MPMS, Quantum Design). The diamagnetism of the sample was taken into account by using Pascal's constants. The Mössbauer spectra were recorded with a conventional Mössbauer spectrometer operating in a constant-acceleration mode and equipped with a ^{57}Co/Rh source at room temperature. The sample was placed in an Oxford bath cryostat. Cyclic voltammetric measurements were carried out by use of PAR equipment (potentiostat M 173; universal programmer M 175) on CH_3CN solutions that contained 0.1 M tetra-*n*-butylammonium hexafluorophosphate ([TBA]PF_6) as supporting electrolyte. $E_{1/2}$ values, determined as $(E_{p,a} + E_{p,c})/2$, were referenced to the Ag/AgCl electrode (saturated LiCl, C_2H_5OH) at ambient temperature and are uncorrected for junction potentials. The ferrocenium/ferrocene (Fc^+/Fc) couple was used as internal standard (≈10^{-3} M). Under our experimental conditions the Fc^+/Fc couple is at $E_{1/2}$ = +0.51 V vs Ag/AgCl.

X-ray Crystallography. The crystallographic data on [LTi]BPh_4 (**1**), **5**, **8**, and **11** are summarized in Table I. A yellow crystal of **1**, a pink crystal of **5**, a red crystal of **8**, and a blue-black crystal of **11** were mounted on a glass fiber and placed on a Syntex R3 or Siemens P4 diffractometer, respectively. Graphite monochromated Mo-Kα X-radiation was used throughout. Unit cell parameters were determined in all cases by the automatic indexing of 25–35 centered reflections. Intensity data were corrected for Lorentz, polarization, and absorption effects (empirical ψ-scans) in the usual manner. The structures were solved by conventional Patterson and difference Fourier methods by using the SHELXTL-PLUS program package.[12] The function minimized during full-matrix least-squares refinement was $\sum w(|F_o| - |F_c|)^2$, where $w = 1/\sigma^2(F)$. Neutral-atom scattering factors and anomalous dispersion correction for non-hydrogen atoms were taken from ref 13a. The positions of the hydrogen atoms of the methylene groups were either placed at calculated positions with group isotropic thermal parameters or found in the final difference Fourier map (**5**). The methyl groups were treated as rigid bodies. All non-hydrogen atoms were refined with anisotropic thermal parameters. Due to the presence of three tertiary butyl groups per metal ion the crystallinity of the crystals was not as good as might be desirable for high-quality X-ray determination. Since **1**, **5**, and **8** crystallize in noncentrosymmetric space groups Roger's[13b] η-factor test and Hamilton's R-test[13c] were carried out in each case. These proved to be inconclusive. Therefore, the structures were fully refined in both enantiomeric forms and the refinement yielding the lower R-value was deemed to be the correct one. Due to weak intermolecular packing forces between the neutral molecules in crystals of **5** and **8** the tertiary butyl groups of L are disordered. For **5** this disorder was successfully modeled by a split atom model. For the carbon atoms of the three methyl groups two positions with 0.33 and 0.66 occupancy were refined, respectively. For **8** this proved not to be possible. Only one position for these methyl carbon atoms was found, but large, physically meaningless anisotropic thermal parameters also indicate some degree of disorder. Atom coordinates for complexes **1**, **5**, **8**, and **11** are listed in Table II.

Results

Syntheses. The hexadentate ligand 1,4,7-tris(5-*tert*-butyl-2-hydroxybenzyl)-1,4,7-triazacyclononane (H_3L) was prepared in good yields as its tripotassium trisphenolate salt, K_3L, by the reaction of 2-bromomethyl-4-*tert*-butylphenyl acetate and 1,4,7-triazacyclononane and KOH in toluene (Scheme II). K_3L was used as starting material for the synthesis of complexes.

Reaction of $TiCl_3$ and K_3L (1:1) in CH_3CN under anaerobic conditions produced a green precipitate which dissolved rapidly again upon exposure of the reaction mixture to air. From the clear solution yellow crystals of diamagnetic $[LTi^{IV}]PF_6$ (**1**) precipitated upon addition of $NaPF_6$. The tetraphenylborate salt was obtained by metathesis reaction in the form of X-ray-quality yellow crystals.

Figure 1 shows the 400-MHz ^{1}H NMR spectrum of **1** in CD_3CN; Table II gives chemical shifts and assignments according to Chart I. The signals h and i are assigned to aromatic protons whereas signal a corresponds to the methyl protons of the *tert*-butyl groups. The proton H_h in the *ortho* position relative to the phenolate oxygen is more strongly shielded than the aromatic protons H_i in the meta position. Consequently, the signal of H_h appears at a higher field than H_i. The signals of the benzylic protons H_f and H_g are shifted to lower fields as compared to the uncoordinated ligand (δ = 3.75) and benzylamine (δ = 3.72). The neighboring titanium(IV) ion obviously induces an additional deshielding. Assignment of the diastereotopic amine methylene protons (H_b, H_c, H_d, H_e) was unambiguously achieved by a series

(12) Full-matrix least-squares structure refinement program package SHELXTL-PLUS: Sheldrick, G. M. (University of Göttingen).

(13) (a) *International Tables of Crystallography*; Kynoch: Birmingham, England, 1974; Vol. IV, pp 99, 149. (b) Roger, D. *Acta Crystallogr.* **1981**, *A37*, 734. (c) Hamilton, W. C. *Ibid.* **1965**, *18*, 502.

Table II. Atomic Coordinates (×10⁴) and Equivalent Isotropic Displacement Parameters (Å² × 10³) for Complexes **1**, **5**, **8**, and **11**

atom	x	y	z	U(eq)	atom	x	y	z	U(eq)	atom	x	y	z	U(eq)
							Compound **1**							
Ti(1)	2468(2)	8412(1)	1041(1)	48(1)	C(42)	1365(9)	7610(5)	1937(4)	54(5)	C(2)	953	10729	8711	90(4)
N(1)	3662(8)	9094(5)	1505(3)	45(4)	C(43)	527(10)	8204(6)	2074(4)	43(4)	C(3)	1897	11212	8648	81(4)
N(2)	2631(9)	7827(4)	1770(3)	44(3)	C(44)	420(11)	8770(6)	1761(4)	51(5)	C(4)	2925	11045	8356	75(4)
N(3)	4285(7)	7894(4)	964(3)	44(3)	C(45)	−356(11)	9307(6)	1879(5)	58(5)	C(5)	3011	10397	8128	63(4)
C(25)	3305(10)	8989(5)	2045(4)	54(5)	C(46)	−1082(11)	9274(6)	2305(5)	63(5)	C(6)	2067	9914	8191	58(3)
C(26)	3252(10)	8226(5)	2171(4)	53(5)	C(47)	−1011(12)	8698(7)	2621(5)	61(5)	C(7)	827(6)	8230(3)	7400(3)	70(4)
C(27)	3342(10)	7182(5)	1647(4)	49(4)	C(48)	−202(11)	8165(6)	2498(4)	51(5)	C(8)	−143	8049	7081	75(4)
C(28)	4525(10)	7378(5)	1379(4)	57(5)	C(49)	−1887(13)	8681(8)	3074(6)	82(6)	C(9)	−1065	8529	6972	76(4)
C(29)	5207(9)	8467(6)	971(4)	55(4)	C(50)	−1749(13)	8026(6)	3389(4)	110(7)	C(10)	−1018	9190	7184	67(4)
C(30)	5005(10)	8933(5)	1434(4)	56(5)	C(51)	−3256(12)	8707(7)	2882(5)	114(8)	C(11)	−48	9370	7503	72(4)
O(1)	2817(6)	9012(3)	525(2)	49(3)	C(52)	−1628(14)	9298(6)	3415(4)	131(8)	C(12)	874	8890	7611	61(3)
O(2)	1103(6)	8797(3)	1329(3)	53(3)	C(53)	4366(10)	7556(5)	458(4)	58(5)	C(13)	4570(8)	9068(3)	7761(2)	65(4)
O(3)	1852(6)	7655(3)	714(2)	49(3)	C(54)	3508(11)	6959(6)	395(4)	45(5)	C(14)	5610	8974	7459	76(4)
C(31)	3374(10)	9835(5)	1389(3)	54(5)	C(55)	2264(13)	7049(6)	515(4)	52(5)	C(15)	5477	8857	6942	74(4)
C(32)	3651(10)	10062(6)	858(4)	51(5)	C(56)	1435(10)	6503(6)	445(4)	55(5)	C(16)	4305	8835	6727	76(4)
C(33)	4087(10)	10721(6)	762(4)	60(5)	C(57)	1854(11)	5890(6)	236(4)	56(5)	C(17)	3265	8929	7029	57(3)
C(34)	4198(11)	10979(6)	277(5)	62(5)	C(58)	3067(13)	5787(7)	105(5)	61(5)	C(18)	3398	9046	7546	57(3)
C(35)	3899(12)	10564(7)	−118(4)	71(6)	C(59)	3892(11)	6324(6)	185(4)	49(4)	C(19)	2885(6)	7882(3)	8281(2)	65(3)
C(36)	3465(10)	9898(6)	−41(4)	58(5)	C(60)	3499(13)	5106(7)	−145(5)	73(6)	C(20)	3135	7400	8658	71(4)
C(37)	3305(11)	9655(6)	447(5)	55(5)	C(61)	2815(14)	5037(6)	−647(4)	125(8)	C(21)	2934	7569	9163	64(4)
C(38)	4588(16)	11732(7)	192(6)	92(7)	C(62)	4849(12)	5101(6)	−264(5)	114(7)	C(22)	2483	8222	9291	72(3)
C(39)	4840(19)	11929(7)	−319(5)	222(15)	C(63)	3185(12)	4512(5)	188(5)	116(7)	C(23)	2232	8705	8913	65(3)
C(40)	5651(18)	11933(7)	499(5)	178(12)	B(1)	2172(11)	9135(6)	7934(4)	53(5)	C(24)	2433	8535	8408	54(3)
C(41)	3617(17)	12192(7)	376(8)	252(16)	C(1)	1038(6)	10081(3)	8482(3)	85(4)					
							Compound **5**							
Cr	0	0	0	29(1)	C(5)	8602(3)	9336(3)	11269(8)	39(3)	C(11)	6457	7838	7635	135(3)
O(1)	9233(2)	9795(2)	11622(5)	37(2)	C(6)	8114(3)	9416(4)	12143(10)	54(3)	C(12)	6062	8168	10958	135(3)
N(1)	9444(3)	9244(3)	7930(7)	39(3)	C(7)	7458(4)	8989(4)	11718(11)	73(4)	C(13)	6370	7311	10820	135(3)
C(1)	9157(4)	9482(4)	6304(9)	50(3)	C(8)	7267(4)	8459(5)	10457(13)	75(4)	C(11′)	6368	8319	8198	125(7)
C(2)	9910(3)	9065(3)	6966(9)	44(3)	C(9)	7760(3)	8372(3)	9605(10)	59(3)	C(12′)	6454	7418	8566	125(7)
C(3)	8925(3)	8667(3)	9074(10)	45(3)	C(10)	6561(3)	7994(4)	9959(12)	103(3)	C(13′)	6149	7620	11857	125(7)
C(4)	8421(3)	8788(3)	10013(8)	44(3)										
							Compound **8**							
Fe(1)	10000	10000	10000	37(1)	C(4)	8386(4)	8781(4)	9712(13)	54(4)	C(9)	7729(4)	8360(4)	9325(15)	69(5)
O(1)	9196(3)	9746(3)	11395(8)	45(3)	C(5)	8573(4)	9325(4)	11028(12)	48(4)	C(10)	6544(7)	7972(10)	9580(32)	132(10)
N(1)	9432(3)	9234(3)	7694(10)	46(3)	C(6)	8074(4)	9375(5)	11851(13)	62(5)	C(11)	6439(8)	7953(15)	7540(28)	483(41)
C(1)	9144(4)	9492(4)	6100(11)	53(5)	C(7)	7423(5)	8951(6)	11466(15)	89(7)	C(12)	6101(7)	8094(10)	10359(38)	342(26)
C(2)	9902(4)	9050(4)	6772(12)	53(4)	C(8)	7243(5)	8433(6)	10176(17)	78(6)	C(13)	6337(9)	7341(9)	10263(45)	344(27)
C(3)	8911(4)	8671(4)	8813(13)	55(5)										
							Compound **11**							
Fe(1)	1183(1)	4991(1)	718(1)	34(1)	C(12)	802(5)	7172(6)	−1045(4)	42(3)	C(29)	1257(5)	6818(6)	1680(4)	43(3)
O(1)	300(3)	5154(4)	1305(3)	40(2)	C(13)	1157(5)	6366(5)	−693(4)	34(3)	C(30)	656(5)	6398(6)	2194(4)	38(3)
O(2)	794(3)	5983(3)	−75(3)	34(2)	C(14)	2158(8)	7582(8)	−2676(6)	86(5)	C(31)	557(5)	6798(6)	2904(4)	47(3)
O(3)	703(3)	3873(3)	181(3)	35(2)	C(15)	3012(9)	7226(11)	−2784(7)	184(10)	C(32)	17(5)	6433(7)	3386(4)	50(3)
N(1)	2344(3)	4994(5)	187(3)	39(2)	C(16)	1596(9)	7476(14)	−3317(5)	293(16)	C(33)	−436(5)	5627(7)	3136(5)	54(3)
N(2)	1891(4)	4015(5)	1464(3)	38(3)	C(17)	2371(9)	8660(10)	−2540(7)	169(9)	C(34)	−367(5)	5206(6)	2439(4)	47(3)
N(3)	1840(4)	6075(5)	1424(3)	38(2)	C(18)	1400(5)	3098(6)	1553(4)	44(3)	C(35)	179(5)	5581(6)	1960(4)	36(3)
C(1)	2726(5)	4022(6)	363(4)	43(3)	C(19)	1337(5)	2514(6)	838(4)	37(3)	C(36)	−68(7)	6858(9)	4150(6)	71(4)
C(2)	2719(5)	3801(6)	1189(4)	46(3)	C(20)	1587(5)	1553(6)	806(4)	43(3)	C(37)	−278(13)	7858(15)	4112(8)	381(22)
C(3)	1972(5)	4556(6)	2202(4)	44(3)	C(21)	1498(5)	989(6)	169(4)	42(3)	C(38)	657(8)	6854(15)	4583(7)	254(15)
C(4)	2282(5)	5586(6)	2077(4)	44(3)	C(22)	1101(5)	1420(6)	−478(4)	42(3)	C(39)	−668(11)	6490(14)	4592(8)	346(17)
C(5)	2410(5)	6552(6)	919(4)	46(3)	C(23)	840(4)	2375(5)	−479(4)	34(3)	Cl(1)	338(2)	10068(4)	2531(2)	113(2)
C(6)	2888(5)	5808(6)	477(4)	45(3)	C(24)	958(5)	2924(5)	177(4)	35(3)	O(11)	904(6)	9351(8)	2387(6)	177(6)
C(7)	2211(4)	5030(7)	−653(3)	43(3)	C(25)	1757(5)	−79(7)	146(5)	52(3)	O(12)	442(8)	10269(11)	3254(6)	213(8)
C(8)	1845(5)	5958(5)	−955(4)	35(3)	C(26)	2155(7)	−316(7)	−577(6)	107(6)	O(13)	−437(6)	9899(10)	2369(8)	231(8)
C(9)	2190(5)	6376(6)	−1582(4)	45(3)	C(27)	2351(7)	−329(7)	800(6)	108(5)	O(14)	534(10)	10964(11)	2244(11)	352(13)
C(10)	1837(5)	7169(6)	−1958(4)	48(3)	C(28)	1025(7)	−709(7)	184(6)	97(5)	O(aq)	5525(17)	5287(22)	664(14)	576(18)
C(11)	1150(5)	7556(6)	−1681(4)	50(3)										

[a] Equivalent isotropic U defined as one-third of the trace of the orthogonalized U_{ij} tensor.

of NOE difference spectra. The N–CH_2–CH_2–N protons of the cyclic amine backbone of the ligand give rise to an ABCD system (Figure 1). A graphical evaluation of this spectrum gives the following estimates for the coupling constants: $|J_{ad}| \approx 0$, $|J_{bd}| \approx 5$ Hz, $|J_{bc}| \approx 13$ Hz, and $|J_{be}| \approx 15$ Hz. An HH-Homo-Cosy spectrum clearly indicates the absence of coupling between protons H_c and H_d. By using the Karplus equation[14] the dihedral angles ϕ_n between the planes defined by H–C(25)–C(26) and H–C(26)–C(25) (Chart I and Figure 2) can be calculated to be 78.9 and 38.5° by using an equatorial–equatorial coupling constant $^3J_{ee} = 0$ Hz and equatorial–axial coupling $^3J_{ae} \approx 5$ Hz, respectively. These values are in reasonable agreement with those in the solid state (75.7°; 43.9°) (see below). Thus the ^{1}H NMR spectrum of **1** clearly shows that the ($\delta\delta\delta$) or ($\lambda\lambda\lambda$) configuration of the three five-membered chelate rings $\overline{\text{Ti–N–C–C–N}}$ is retained in solution on the time scale of an NMR experiment; no fluctional behavior is observed at room temperature.

Since the cation in **1** possesses C_3 symmetry, 13 resonances for the carbon atoms are expected in the ^{13}C NMR spectrum. This reduces to 11 because the methyl carbon atoms of the *tert*-butyl groups are magnetically equivalent. These 11 signals are observed (Table III). From DEPT and CH-Hetero-COSY experiments all resonances with the exception of two aromatic ring carbon atoms H and I could be assigned as in Table III and Chart I.

Reaction of VCl_3 and K_3L (1:1) in acetonitrile under anaerobic conditions provides crystalline green [LV^{III}] (**2**) in 96% yield. Solutions of **2** in CH_3CN are stable in the presence of air but absence of protons for days. Addition of a few drops of concentrated $HClO_4$ to such a solution induced a rapid color

(14) Karplus, M. *Chem. Phys.* **1959**, *30*, 11.

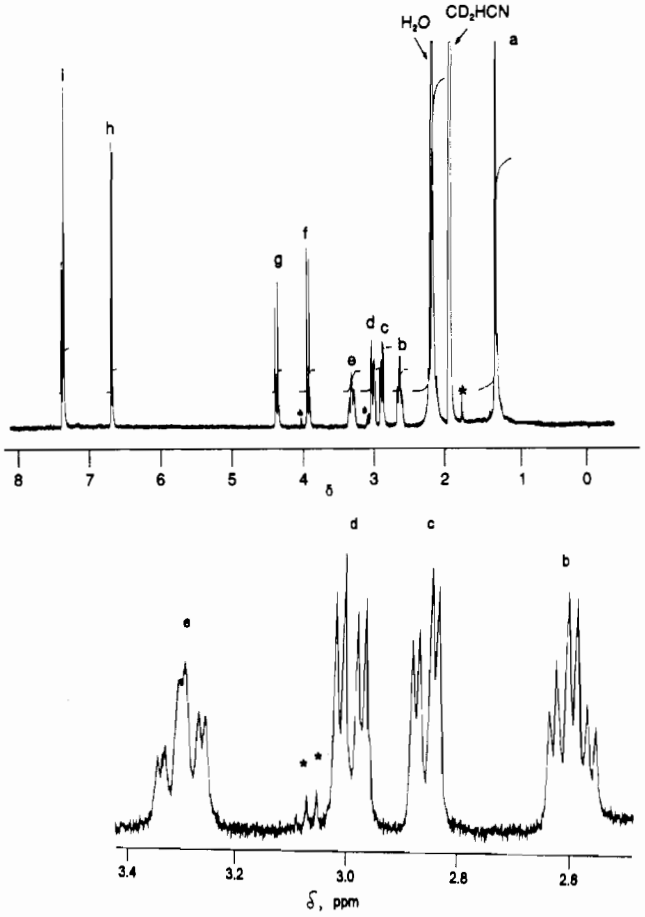

Figure 1. 400-MHz ^{1}H-NMR spectrum of $[LTi^{IV}](PF_6)$ in CD_3CN (top) and methylene proton signals in the region δ = 3.4–2.6 ppm (bottom). Asterisks mark unknown impurities.

Chart I

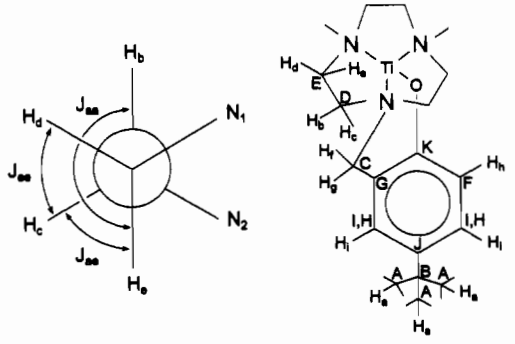

change from green to violet in the presence of air, and violet crystals of $[LV^{IV}](ClO_4)$ (**3**) were obtained. **3** does not contain a V^{IV}=O group as was judged from the absence of a ν(V=O) stretching frequency (930–980 cm^{-1}) in the infrared and a crystal structure determination of $[LV]BPh_4$ (see below). Interestingly, **3** was also obtained from a refluxing methanolic solution of $VO(SO_4)\cdot H_2O$ and K_3L to which a few drops of concentrated $HClO_4$ had been added. Thus, the hexadentate ligand L^{3-} is capable of displacing a terminal oxo group in the presence of protons.

When the above air oxidation of **3** was carried out in strongly acidic methanolic medium, the color of the solution changed from green to violet and, finally, to deep blue. From such a solution blue-black crystals of $[LV^{V}](ClO_4)_2$ (**4**) precipitated. Complex **4** is diamagnetic in agreement with a d^0 electronic configuration. The absence of strong bands in the 800–980-cm^{-1} region in infrared indicates the absence of V^{V}=O or $V^{V}(O)_2$ groups. **4** was also obtained from an acidic acetonitrile solution of $(NH_4)VO_3$ and

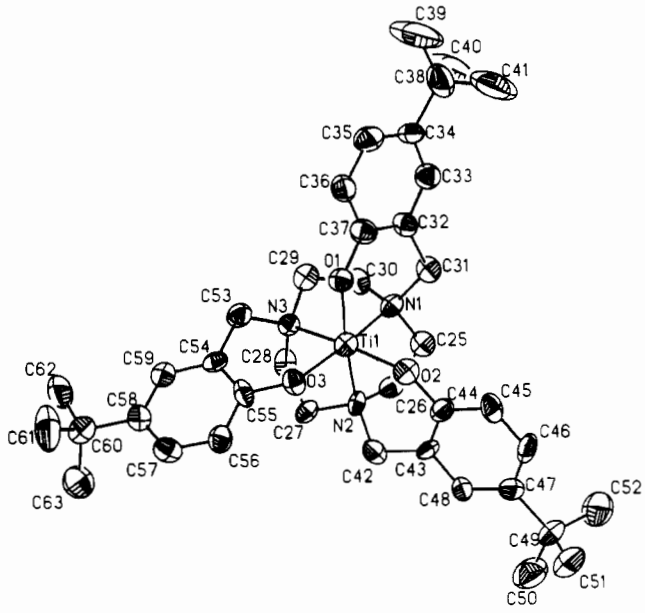

Figure 2. Perspective view and atom labeling of the monocation in crystals of $[LTi^{IV}]BPh_4$.

Table III. 400-MHz ^{1}H NMR and ^{13}C NMR Data for $[LTi]PF_6$ (**1**) in CD_3CN

	signal	δ, ppm	integration	assgnt[a]
^{1}H NMR	singlet	1.30	27 H	a
	doublet of triplets	2.65	3 H	b
	doublet of doublets	2.90	3 H	c
	doublet of doublets	3.05	3 H	d
	doublet of triplets	3.35	3 H	e
	doublet	3.95	3 H	f
	doublet	4.35	3 H	g
	doublet	6.65	3 H	h
	multiplet	7.35	6 H	i
^{13}C NMR		31.6		A
		35.0		B
		52.3		C
		62.6		D
		64.7		E
		115.1		F
		124.9		G
		128.2		H or I
		128.7		I or H
		147.0		J
		159.1		K

[a] See Chart I for proton and carbon labels.

K_3L. This result stresses again the extraordinary coordinating capability of the ligand L^{3-}.

Octahedral chromium(III) complexes are usually quite robust. In accord with this notion is the observation that $CrCl_3\cdot 6H_2O$ in a variety of solvents does not react with K_3L. Addition of activated zinc, which produces labile chromium(II) intermediates, to such a CH_3CN solution induced rapid formation of pink $[LCr^{III}]$ (**5**).

The green neutral complex $[LMn^{III}]$ (**6**) was obtained in 96% yield from a methanolic solution of K_3L and $Mn_3^{III}(\mu\text{-}O)(OAc)_7(HOAc)$ (3:1). A methanolic solution of **6** which was acidified by addition of $HClO_4$ reacted in the presence of air yielding a deep blue solution from which upon addition of $NaBPh_4$ blue crystals of $[LMn^{IV}]BPh_4$ (**7**) precipitated.

Reaction of $Fe(ClO_4)_3\cdot 6H_2O$ and K_3L in methanol produced red crystals of $[LFe^{III}]$ (**8**) in quantitative yield. The enormous stability of **8** is nicely demonstrated by the following experiments. (i) To a solution of **8** (0.10 g) in a methanol/water mixture (10:1; 50 mL) was added NaOH (1.0 g) which resulted in a pH of ≈13. Even after reflux of this solution for 6 days, no degradation of **8** or precipitation of $Fe(OH)_3$ was detected. (ii) In contrast, when to a suspension of freshly precipitated $Fe^{III}(OH)_3$ (0.10 g)

in methanol (50 mL) was added K_3L (0.80; 0.11 mmol) and the solution was heated to reflux for 3 d, quantitative formation of **8** was observed.

Green [LCo^{III}] (**9**) was obtained in quantitative yield from a solution of $Co(ClO_4)_2 \cdot 6H_2O$ and K_3L (1:1) in acetone/triethylamine in the presence of air.

Most of the neutral complexes [LM] were found to be sparingly soluble in polar organic solvents and insoluble in water. Addition of perchloric acid to suspensions of [LM] (M = Cr, Fe, Co) in methanol at ambient temperature facilitated the solubility of these species. Clear solutions were obtained from which crystalline materials precipitated slowly. These analyzed as $[(LH)M](ClO_4) \cdot H_2O$. Thus, protonation of neutral molecules had occurred. As we will show below, one of the coordinated phenolate ligand arms is protonated and two such monocations form a hydrogen-bonded dimer: $[(LH)_2M^{III}_2](ClO_4)_2 \cdot 2H_2O$ (M = Cr (**10**), Fe (**11**), Co (**12**)).

It is not possible to protonate the mono- or dicationic species $[LM]^{n+}$ (M = Ti^{IV}, V^{IV}, Mn^{IV}, V^{V}) in acidic solutions (1.0 M $HClO_4$). The basicity of the coordinated phenolate groups is obviously greatly reduced in these complexes as compared to their neutral LM (Cr, Fe, Co) counterparts. This is most probably due to relatively strong d_π–p_π bonding in the Ti^{IV}, V^{IV}, Mn^{IV}, and V^{V} species.

Crystal Structures. Crystallographic data for [LTi]BPh_4 (**1**), [LCr] (**5**), [LFe] (**8**), and $[(LH)_2Fe_2](ClO_4)_2 \cdot 2H_2O$ (**11**) are summarized in Table I; Table IV gives selected bond distances and angles. Since the monomeric complexes in crystals of **1**, **5**, and **8** are isostructural, we show only one representative view of such complex in Figure 2. The crystal structure of [LV]BPh_4 (**3**) has been communicated previously.[10]

3 and **1** are isostructural and isomorphous as are **5** and **8**. The latter two crystallize in the acentric space group $R3$. The neutral molecules possess crystallographically imposed C_3 symmetry whereas the monocations in **1** and **3** do not possess crystallographic symmetry. The stereochemistry of the monocations in **1** and **3** and of the neutral molecules in **5** and **8** is very similar (C_3 symmetry). In each case the transition metal is in a pseudooctahedral environment which is composed of three facially coordinated amine nitrogen atoms and three phenolate oxygen atoms. The three five-membered M–N–C–C–N chelate rings of the 1,4,7-triazacyclononane backbone have ($\lambda\lambda\lambda$) or ($\delta\delta\delta$) configuration. In **5** and **8** spontaneous resolution of the two enantiomers by crystallization is observed as is for **1** and **3**.

The three phenolate pendant arms form three six-membered chelate rings which are symmetry related by a C_3 axis. Consequently, these rings can adopt either Λ or Δ- configuration in an octahedral polyhedron. In the present series of complexes the absolute configuration is $\Lambda(\delta\delta\delta)$ or $\Delta(\lambda\lambda\lambda)$.

In the following we compare stereochemical and metrical details of the N_3O_3M skeleton of complexes as a function of the d^n electronic configuration of the central metal ion and the overall charge of the complex (0 or +1).

[LTi^{IV}]. The average Ti–OAr metal-to-oxygen distance of 1.828 Å is short and agrees well with those found in other alkoxy- or (aryloxy)titanium(IV) species[15] (1.79–1.86 Å). For a Ti–OAr single bond, distances between 1.93 and 2.10 Å have been predicted.[15] From the sum of Shannon's ionic radii[16] a distance of 1.96 Å is calculated. These considerations indicate considerable Ti–O double-bond character in **1** despite the fact that the average Ti–O–C bond angle deviates considerably from linearity (average 139.9°). Although there is a steric component to this angle, it also reflects to a certain degree the amount of oxygen p to metal d π bonding that takes place at the Lewis acidic Ti(IV) center.

(15) (a) Latesky, S. L.; Keddington, J.; McMullen, A. E.; Rothwell, I. P.; Huffman, J. C. *Inorg. Chem.* **1985**, *24*, 995. (b) Jones, R. A.; Hefner, J. G.; Wright, T. C. *Polyhedron* **1984**, *3*, 1121.

(16) Shannon, R. D. *Acta Crystallogr.* **1976**, *A32*, 751.

Table IV. Selected Bond Distances (Å) and Angles (deg) for [LTi]BPh_4 (**1**), [LCr] (**5**), [LFe] (**8**), and $[Fe_2(LH)_2](ClO_4)_2 \cdot 2H_2O$ (**11**)

1

Ti–N(1)	2.221(9)	Ti–O(1)	1.833(6)
Ti–N(2)	2.244(8)	Ti–O(2)	1.824(7)
Ti–N(3)	2.222(8)	Ti–O(3)	1.828(7)
O(1)–C(37)	1.368(14)	O(3)–C(55)	1.360(13)
O(2)–C(44)	1.366(13)		
N(1)–Ti–N(2)	77.1(3)	O(1)–Ti–O(2)	102.8(3)
N(1)–Ti–N(3)	78.5(3)	N(1)–Ti–O(3)	162.1(3)
N(2)–Ti–N(3)	77.4(3)	N(2)–Ti–O(3)	91.9(3)
N(1)–Ti–O(1)	85.2(3)	N(3)–Ti–O(3)	85.5(3)
N(2)–Ti–O(1)	160.8(3)	O(1)–Ti–O(3)	103.2(3)
N(3)–Ti–O(1)	91.9(3)	O(2)–Ti–O(3)	103.1(3)
N(1)–Ti–O(2)	90.1(3)	Ti–O(1)–C(37)	140.2(7)
N(2)–Ti–O(2)	84.9(3)	Ti–O(2)–C(44)	140.8(7)
N(3)–Ti–O(2)	160.6(3)	Ti–O(3)–C(55)	138.8(7)

3

V–O	1.825(5)	V–N	2.168(6)
O–C	1.356(9)		
O–V–O	100.0(2)	N–V–N	79.8(2)
O–V–N_t	165.5(2)	O–V–N_c	90.1(2)
V–O–C	136.8(5)		

5

Cr–O	1.937(5)	Cr–N	2.083(5)
O–C	1.326(7)		
O–Cr–O	93.1(2)	O–Cr–N_c	92.8(3)
N–Cr–N	82.9(2)	O–Cr–N_t	172.7(2)
Cr–O–C	129.5(4)		

8

Fe–O	1.918(6)	Fe–N	2.229(6)
O–C	1.323(8)		
O–Fe–O	98.9(2)	O–Fe–N_c	88.5(2)
N–Fe–N	78.5(2)	Fe–O–C	134.7(5)
O–Fe–N_t	165.3(2)		

11

Fe(1)–O(1)	1.861(5)	Fe(1)–N(1)	2.190(6)
Fe(1)–O(2)	2.041(5)	Fe(1)–N(2)	2.177(6)
Fe(1)–O(3)	1.954(5)	Fe(1)–N(3)	2.194(6)
O(1)–C(35)	1.334(9)	O(2)···O(3b)	2.470(10)
O(2)–C(13)	1.392(9)	O_w···O_w(a)	2.950(12)
O(3)–C(24)	1.374(9)	O_w···O(12)	2.582(10)
O(1)–Fe(1)–O(2)	95.0(2)	O(1)–Fe(1)–N(1)	168.7(2)
O(2)–Fe(1)–O(3)	95.1(2)	O(2)–Fe(1)–N(1)	86.7(2)
O(1)–Fe(1)–O(3)	93.7(2)	O(3)–Fe(1)–N(1)	97.3(2)
N(1)–Fe(1)–N(2)	79.4(2)	O(1)–Fe(1)–N(2)	98.0(2)
N(1)–Fe(1)–N(3)	80.5(2)	O(2)–Fe(1)–N(2)	165.8(2)
N(2)–Fe(1)–N(3)	81.1(2)	O(3)–Fe(1)–N(2)	89.8(2)
Fe(1)–O(1)–C(35)	135.4(5)	O(1)–Fe(1)–N(3)	88.3(2)
Fe(1)–O(2)–C(13)	132.2(4)	O(2)–Fe(1)–N(3)	93.6(2)
Fe(1)–O(3)–C(24)	129.6(4)	O(3)–Fe(1)–N(3)	170.9(2)

It is noted that this angle is larger than in any other complex of the present series. It is also noted that the average O–Ti–O bond angle in **1** of 103.0° is the largest in the series. In the extreme case it is possible to envisage a total of four electrons being donated by a phenolate group (three Ti=O–R double bonds), which renders $[LTi^{IV}]^+$ an 18-electron species.

[LV^{IV}]$^+$. This complex contains one more electron (d^1) than $[LTi^{IV}]^+$. The ionic radius of V(IV) in an octahedral environment is smaller by 0.02 Å than the one of Ti(IV).[16] Since the average V–OR distance is observed at 1.825 Å which is smaller by only 0.003 Å than the corresponding Ti–OR distance in **1**, we conclude that the V–O d_π–p_π double-bond character in **3** is slightly less

Table V. Comparison of Structural Data for Octahedral Phenolate Complexes

complex[d]	M–O_{calcd}, Å[c]	av M–O exp, Å	Δ_1, Å[a]	M–N_{calcd}, Å[c]	av M–N_{exp}, Å	Δ_2, Å[b]	ref
$[Ga^{III}(txtacn)]H^+$	1.97	1.94	0.03	2.08	2.11	–0.03	2
$[Ti^{IV}L]^+$	1.96	1.83	0.13	2.07	2.23	–0.16	this work
$[V^{III}(BBPEN)]^+$	1.99	1.89	0.10	2.10	2.23	–0.13	42
$[V^{IV}L]^+$	1.93	1.83	0.10	2.04	2.17	–0.13	this work
$[Cr^{III}L]$	1.97	1.94	0.03	2.08	2.08	0.00	this work
$[Fe^{III}L]$	2.00	1.92	0.08	2.11	2.23	–0.12	this work

[a] Δ_1 = difference of distance $(M–O)_{calcd} - (M–O)_{exp}$. [b] Δ_2 = difference of distance $(M–N)_{calcd} - (M–N)_{exp}$. [c] Sum of ionic radii: Shannon, R. D. *Acta Crystallogr.* **1976**, *A32*, 751. [d] Ligand abbreviations: txtacn = 1,4,7-tris(3,5-dimethyl-2-hydroxybenzyl)-1,4,7-triazacyclononan; BBPEN = *N,N'*-bis(2-hydroxybenzyl)-*N,N'*-bis(2-methylpyridyl)ethylenediamine.

pronounced. This is in accord with the observation that the average O–V–O bond angle of 100.0° is a little smaller in **3** than in **1**.

[LCr^{III}]. This is the first neutral LM compound of the present series. It contains a chromium(III) metal ion with a half-filled t^3_{2g} valence subshell. A comparison of the measured Cr–O distance of 1.931(6) Å with the sum of the ionic radii of 1.97 Å shows that d_π–p_π bonding cannot be important. The O–Cr–O bond angle of 93.1° is close to the ideal octahedral angle of 90°; it is smaller by 10° than in $[LTi^{IV}]^+$ (and by 6.9° than in $[LV^{IV}]^+$).

Furthermore, the Cr–N distance of 2.083(5) Å is within experimental error identical with Cr(TCTA),[17] where TCTA represents the ligand 1,4,7-triazacyclononane-1,4,7-trisacetate. It is also pertinent that the sums of the ionic radii for Cr^{III}–N and Cr^{III}–O are 2.08 and 1.97 Å, respectively. Clearly the Cr–O bonds do not exert a structural trans influence on the Cr–N bonds in trans position. In contrast, the Ti^{IV}–N and V^{IV}–N bonds in **1** and **3** are significantly longer than predicted from Shannon's ionic radii (Table V).

[LFe^{III}]. **8** contains a high-spin ferric ion with a $t^3_{2g}e_g^2$ electronic configuration. The Fe–O distance in **8** is short (1.918 Å), indicating some oxygen-to-iron π bonding; it is much shorter than in Raymond's tris(catecholato)iron(III) complex, $[Fe(cat)_3]^{3-}$ (Fe–O: 2.015(6) Å),[18] but in accord with other (phenolato)-iron(III) complexes: [Fe(salen)(ox)]$^-$, 1.914 Å,[19] [Fe(salen)-(acac)], 1.899 and 1.958 Å; [Fe(salen)(PSQ)], 1.916 Å;[20] [Fe(*o*-tatp)], 1.889 Å[3]. The Fe–O distance in **8** is significantly shorter than the sum of the ionic radii (2.00 Å) and in $Fe(acac)_3$ (1.992 Å),[21] $Fe(trop)_3$ (2.008 Å),[22] and $Fe(cupferron)_3$ (2.00 Å),[23] where typical Fe–O single bonds prevail. The O–Fe–O angle at 98.9° is larger than in **5** but smaller than in **1** or **3**. The Fe–O–C bond angle increases by 5.2° as compared to **5** allowing better overlap of an oxygen p orbital with an iron d orbital. On the other hand, the Fe–N bond distances are not affected by the phenolate-to-iron bonds in trans position; no structural trans influence has been detected. Thus **8** is probably best described as a species with weak d_π–p_π phenolate-to-iron bonds. It resembles in many aspects **5** rather than **1** and **3**. The features of the N_3O_3Fe core described here are virtually identical in FeL″ (L″ = 1,4,7-tris-(3-*tert*-butyl-2-hydroxybenzyl)-1,4,7-triazacyclononane).[3] Thus shifting the position of the *tert*-butyl group at the aromatic ring does not influence the metrical details of the N_3O_3Fe polyhedron.

[CoL′]. We have not been able to grow crystals of **9** suitable for X-ray crystallography. The central cobalt(III) ion has a filled t^6_{2g} electronic configuration, and d_π–p_π bonding is not expected to play a role. Co^{III}–$O_{phenolate}$ distances are found to be in the range 1.89–1.92 Å.[24]

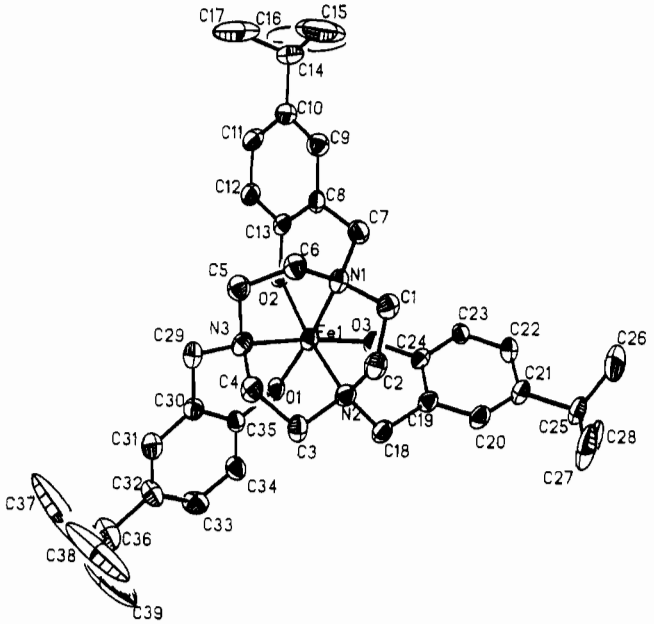

Figure 3. Perspective view and atom labeling of the one crystallographically independent half of the cation in crystals of $[(LH)_2Fe_2](ClO_4)_2 \cdot 2H_2O$.

$[(LH)_2Fe_2](ClO_4)_2 \cdot 2H_2O$. Figure 3 shows the structure and atom-labeling scheme of half of the dimeric dication in crystals of **11**; Figure 4 shows a ball-and-stick representation of the dimer (top) and a schematic drawing of the first coordination spheres and the two hydrogen-bonding contacts (bottom).

In contrast to the neutral molecule in [LFe] the Fe–O bonds in **11** are not equivalent: The Fe–O(1) distance is quite short, Fe–O(3) is medium, and Fe–O(2) is rather long (Table IV). This is a clear structural indication that the proton of the two O(2)–H···O(3) contacts (O(2)···O(3) = 2.470 Å) per dimer, which has not been located, is more closely bound to O(2) than O(3) (asymmetric O–H···O bonding). Interestingly, in a similar alkoxy-bridged dinuclear complex $[CoLH_3LCo]^{3+}$, where L represents 1,4,7-tris[(2*S*)-2-hydroxypropyl]-1,4,7-triazacyclononane, all three coordinated alkoxy groups form O–H···O hydrogen-bonding contacts (O–H···O = 2.481(8) Å).[25] The water molecules of crystallization do not form hydrogen-bonding contacts to the dimer. There is one O–H···O contact to the perchlorate anion at 2.582 Å and a rather weak interaction at 2.950 Å between two such water molecules.

The chromium(III) analogue **10** is isostructural; it crystallizes in the same space group as **11** with very similar unit cell parameters: monoclinic space group $P2_1/n$ with a = 16.50(1) Å, b = 13.83(1) Å, c = 17.73(1) Å, β = 93.66(6)°, and Z = 2. The intradimer Cr···Cr distance is 4.69(1) Å. This has been established

(17) Weighardt, K.; Bossek, U.; Chaudhuri, P.; Herrmann, W.; Menke, B. C.; Weiss, J. *Inorg. Chem.* **1982**, *21*, 4308.
(18) Raymond, K. N.; Isied, S. S.; Brown, L. D.; Fronczek, F. R.; Nibert, J. H. *J. Am. Chem. Soc.* **1976**, *98*, 1767.
(19) Malfant, I.; Morgenstern-Baderau, I.; Philoche-Levisalles, M.; Lloret, F. *J. Chem. Soc., Chem. Commun.* **1990**, 1338.
(20) Lauffer, R. B.; Heistand, R. H.; Que, L., Jr. *Inorg. Chem.* **1983**, *22*, 50.
(21) Iball, J.; Morgan, C. H. *Acta Crystallogr.* **1967**, *23*, 239.
(22) Hamor, T. A.; Watkin, D. J. *J. Chem. Soc., Chem. Commun.* **1969**, 440.
(23) van der Helm, D.; Merritt, K. L.; Degeilh, R.; MacGillavry, C. H. *Acta Crystallogr.* **1965**, *18*, 355.
(24) Riley, P. E.; Pecoraro, V. L.; Carrano, C. J.; Raymond, K. N. *Inorg. Chem.* **1983**, *22*, 3096.
(25) Belal, A. A.; Farrugia, L. J.; Peacock, R. D.; Robb, J. *J. Chem. Soc., Dalton Trans.* **1989**, 931.

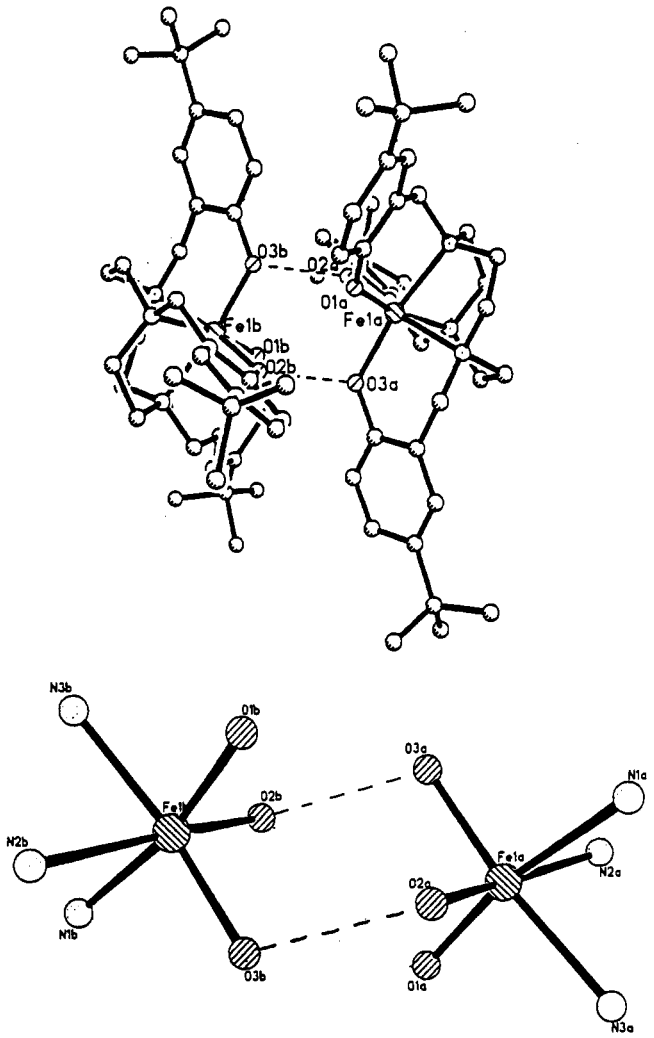

Figure 4. Ball-and-stick representation of hydrogen-bonded dimer in **11** (top) and a representation of the first coordination sphere at the iron(III) centers (bottom) emphasizing the two intramolecular O–H···O hydrogen-bonding contacts.

Table VI. Electrochemistry of Complexes[a]

complex	$E_{1/2}$, V vs Fc^+/Fc	electrode	solvent
(**1**)PF_6	−1.52 r	glassy carbon	CH_3CN
2, **3**, **4**	+0.38 r, −0.50 r, −2.41 r	glassy carbon	CH_3CN
5	+0.30 qr	Pt-button	CH_2Cl_2
6	−0.25 r, −0.88 r	glassy carbon	CH_3CN
8	−1.72 qr	glassy carbon	CH_2Cl_2

[a] Cyclic voltammetry at 22 °C: 0.10 M tetra-*n*-butylammonium hexafluorophosphate supporting electrolyte; 10^{-3} M ferrocene internal standard; reference electrode Ag/AgCl (saturated LiCl in C_2H_5OH); scan rates 20–200 m Vs^{-1}; r = reversible; qr = quasi-reversible.

from a single-crystal X-ray diffraction study, where the structure of **10** has been solved and refined to an *R*-factor of 0.12. The quality of the crystals was low, and we refrain from publication of the full data here.

Electrochemistry. Table VI gives electrochemical data for the complexes. Cyclic voltammograms (cv) on acetonitrile (or CH_2Cl_2) solutions containing 0.10 M tetra-*n*-butylammonium hexafluorophosphate as supporting electrolyte and $\approx 10^{-3}$ M complex have been recorded in the range 1.3 to −2.0 V vs Ag/AgCl with scan rates 20–200 mV s^{-1}. The cv's of **2**–**4** have been reported previously.[10] $[LV^{II}]^-$, $[LV^{III}]$, $[LV^{IV}]^+$, and $[LV^V]^{2+}$ are the electrochemically reversibly accessible oxidation states. **1** and **8** are reversibly reduced at quite negative redox potentials. These data clearly emphasize that the trisphenolato ligand L^{3-} stabilizes higher oxidation states of first-row transition metals. The manganese species $[LMn^{III}]$ (**6**) is reversibly reduced and oxidized by one electron, respectively, eq 1. Interestingly, the complex $[LCr^{III}]$ (**5**) is electrochemically quasi-reversibly oxidized by one electron yielding presumably a chromium(IV) species $[LCr^{IV}]^+$. We have not been able to isolate and characterize this species.

$$[LMn^{IV}]^+ \underset{-e^-}{\overset{+e^-}{\rightleftarrows}} [LMn^{III}] \underset{-e^-}{\overset{+e^-}{\rightleftarrows}} [LMn^{II}]^- \qquad (1)$$

Magnetic Properties and ESR and Mössbauer Spectra. Temperature-dependent molar susceptibility measurements of powdered samples of the mononuclear neutral complexes **1**–**9** have been carried out in the temperature range 80–298 K. The results are summarized in Table VII. **1** and **4** are diamagnetic in accord with a d^0 electronic configuration; **9** is also diamagnetic in agreement with the presence of low-spin cobalt(III) (d^6). **2**, **3**, and **5**–**8** have temperature-independent magnetic moments characteristic of a d^2, d^1, d^3, d^4 high-spin, d^3, and d^5 high-spin electronic configuration, respectively. In contrast, the dimers **10** and **11** exhibit temperature-dependent magnetic moments in the range 2–293 K (Figures 5 and 6). In both cases the magnetic moments drop drastically below 50 K indicating $S = 0$ ground states. At room temperature magnetic moments of 3.7 μ_B/Cr for **10** and 5.9 μ_B/Fe for **11** are observed. Thus intradimer antiferromagnetic spin exchange coupling is observed.

By using the isotropic spin exchange coupling model (Heisenberg, Dirac, van Vleck) with the spin Hamiltonian $H = -2JS_1 \cdot S_2$ [26] ($S_1 = S_2 = {}^3/_2$ for **10** and ${}^5/_2$ for **11**, we have calculated the following spin exchange coupling constants: **10**, $J = -0.93$ cm^{-1} ($g = 1.98$); **11**, $J = -0.33$ cm^{-1} ($g = 1.98$). The best least-squares fits are shown in Figures 5 and 6. We realize that the model used here is probably an oversimplification since zero-field splitting terms cannot be ignored if $|J| < 1$ cm^{-1}. Consequently, the derived absolute values of J should not be taken too seriously.

Figure 7 shows solid-state X-band ESR spectra of **10** at 2.7 and 36.8 K. The relative intensities of "lines" in the spectra of the dimer are significantly temperature-dependent. In particular, the relative amplitudes of the signals at $g \approx 2.2$, 3.8, and 8.0 increase with increasing temperature. Interestingly, a 1:2 ratio of the energies of the signals at $g \approx 3.8$ and 8.0 is observed, which indicates transition $S = 2$ ($-6J$) and $S = 3$ ($-12J$) multiplets. In first order, the Boltzmann population of the multiplet in which the resonance occurs is proportional to the ESR intensity I times temperature T as in eq 2. Here $E(i)$ is the energy of the resonating

$$IT \approx \exp(-E(i)/kT)/Z \qquad (2)$$

multiplet i and Z is the partition function of the system. We adopt an antiferromagnetic exchange interaction and energy separations of $2J$, $6J$, and $12J$, between the spin manifolds, $S = 0$, 1, 2, and 3 with negligible zero-field splittings of the local $S = {}^3/_2$ spin states. Substituting the corresponding partition function $Z = 1 + 3\exp(-2J/kT) + 5\exp(-6J/kT) + 7\exp(-12J/kT)$ and the energies $E(2) = 6J$ and $E(3) = 12J$ for the excited $S = 2$ and $S = 3$ spin multiplets, respectively, in eq 2 and fitting the relative amplitudes of the signals at $g \approx 3.8$ and 8.0 yielded $J = -1.3$ cm^{-1} in reasonable agreement with the susceptibility data. The ESR spectrum of **10** agrees nicely with the one reported by Glerup and Weihe for $[(NH_3)_5CrC{\equiv}NCr(NH_3)_5](ClO_4)_5 \cdot 4H_2O$ ($J = -32.3$ cm^{-1}).[27]

The magnitude of the antiferromagnetic coupling in hydrogen-bonded chromium(III) dimers has recently been shown to be primarily governed by the intradimer Cr···Cr distance according to eq 3,[28] where J is in cm^{-1} and R in Å; $J_0 = 1.97 \times 10^5$ and $a = 2.26$. By using the experimentally determined Cr···Cr distance of 4.69 Å, the calculated value of J is -2.4 cm^{-1}.

(26) O'Connor, C. J. *Prog. Inorg. Chem.* **1982**, *29*, 203.
(27) Glerup, J.; Weihe, H. *Acta Chem. Scand.* **1991**, *45*, 444.
(28) Bossek, U.; Weighardt, K.; Nuber, B.; Weiss, J. *Angew. Chem., Int. Ed. Engl.* **1990**, *29*, 1055.

Table VII. UV–Vis Data and Magnetic Properties of the Complexes[a]

complex	solvent	λ_{max}, nm (ϵ, L mol^{-1} cm^{-1})	μ_{eff}(298 K), μ_B
1	CH_3OH	238 (1.94 × 10^4), 356 (1.62 × 10^4)	diamagnetic
2	CH_3CN	273 (1.74 × 10^4), 360 (4.55 × 10^3), 540 (3.70 × 10^3)	2.8
3	CH_3CN	266 (1.33 × 10^4), 310 sh, 430 (7.2 × 10^3), 553 (9.53 × 10^3)	1.71
4	CH_3CN	296 sh, 327 (1.31 × 10^4), 719 (3.74 × 10^4)	diamagnetic
5	DMF	283 (3.0 × 10^4), 350 sh, 431 (220), 569 (410)	4.0
6	CH_3CN	290 (1.36 × 10^4), 373 (4.08 × 10^3), 629 (895)	4.70
7	CH_3CN	278 (1.65 × 10^4), 330 sh, 400 (4.84 × 10^3), 640 (7.07 × 10^3)	3.83
8	CH_3CN	237 (1.72 × 10^4), 285 (8.63 × 10^3), 320 sh, 486 (4.86 × 10^3)	5.5
9	CH_3CN	254 (3.35 × 10^4), 280 sh, 377 (1.9 × 10^3), 562 (815)	diamagnetic
10[b]	DMF/$HClO_4$	288 (1.5 × 10^4), 365 sh, 548 (400)	af; see text
11[b]	CH_3CN/$HClO_4$	280 (6.9 × 10^3), 326 (3.6 × 10^3), 550 (3.27 × 10^3)	af; see text
12[b]	CH_3CN/$HClO_4$	~280 (1.3 × 10^4), 350 (1.6 × 10^3), 470 (1.05 × 10^3), 660 (490)	diamagnetic

[a] Abbreviations: DMF = dimethylformamide, af = antiferromagnetic spin exchange coupling, and sh = shoulder. [b] Molar absorption coefficients are per dinuclear unit.

Table VIII. Comparison of Structural Data for the Phenolate Complexes

complex[a]	r, Å[b]	α, deg[c]	β, deg[c]	ref
$[Ga(txtacn)]H^+$	0.62	130.5	89.5	2
$[TiL]^+$	0.61	139.9	103.0	this work
$[VL]^+$	0.59	136.8	100.0	this work
$[CrL]^+$	0.62	129.5	93.1	this work
$[FeL]^+$	0.65	134.7	98.9	this work
$L''WO_3 \cdot 3H_2O$	0.58		106.8	40
$[L'''ReO_3]^+$	0.57		102.7	41

[a] Ligand abbreviations are as in Table IV; L'' = 1,4,7-trimethyl-1,4,7-triazacyclononane; L''' = 1,4,7-triazacyclononane. [b] Ionic radius of metal ion with 6-coordination.[16] [c] Angles are defined as in Chart II.

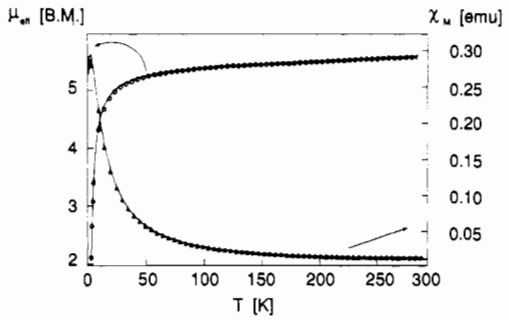

Figure 5. Plots of the molar magnetic susceptibility χ_M and magnetic moment, μ/μ_B, vs. temperature for **10**. Δ and O represent experimental data points; the lines are a least-squares best fit of the data.

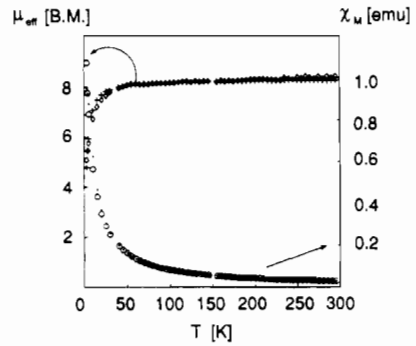

Figure 6. Plots of the molar magnetic susceptibility χ_M and magnetic moment, μ/μ_B, vs. temperature for **11**. + and O represent experimental data points; ◊ and ● are calculated by a least-squares best fit.

$$J = J_0 e^{-aR} \qquad (3)$$

The Mössbauer spectrum recorded without applied external magnetic field of solid **8** at 4.2 K consists of a symmetric quadrupole doublet with an isomer shift of $\delta = 0.38$ mm s^{-1} and a quadrupole splitting of $\Delta E_Q = 0.55$ mm s^{-1}. The isomer shift is within the range $0.3 < \delta < 0.6$ mm s^{-1} observed for a wide variety of mononuclear octahedral high-spin ferric complexes.[29]

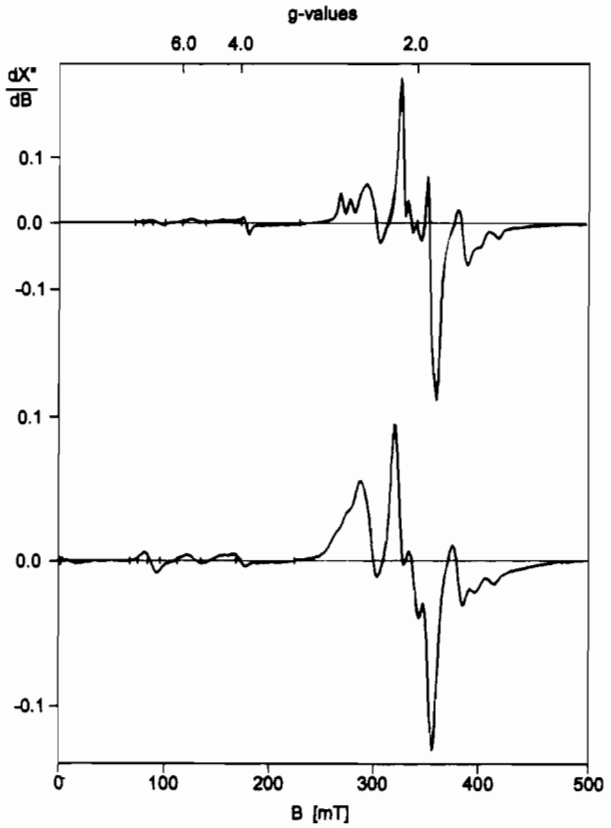

Figure 7. Solid-state X-band ESR spectra of **10** at 2.7 K (top) and 36.8 K (bottom) (9.437-GHz microwave frequency).

The corresponding spectrum of **11** also consists of a symmetric doublet ($\delta = 0.51(2)$ mm s^{-1}; $\Delta E_Q = 1.01(1)$ mm s^{-1}). The fact that only one symmetrical doublet is observed is in agreement with the structure determination which shows that both iron(III) centers of the dinuclear cation in **11** are equivalent. The significantly larger quadrupole splitting in the spectrum of **11** as compared to **8** implies that the iron ions in **11** are in a less symmetrical ligand environment than those in **8**. This is in agreement with the crystal structure determinations.

Electronic Spectra. Table VII summarizes the UV–vis spectral data and magnetic properties of complexes. The uncoordinated trisphenolate ligand K_3L exhibits an intense absorption maximum at 285 nm ($\epsilon = 7.9 \times 10^3$ L mol^{-1} cm^{-1}), which is assigned to an aromatic π–π^* transition. $[LTi^{IV}]^+$—a d^0 system—shows two very intense absorption maxima at 238 and 356 nm with molar absorption coefficients $>10^4$ L mol^{-1} cm^{-1}. The latter absorption may intuitively be assigned to a ligand-to-metal charge transfer in agreement with Raymond's tris(catecholato)titanium(IV)

(29) Murray, K. S. *Coord. Chem. Rev.* **1974**, *12*, 1.

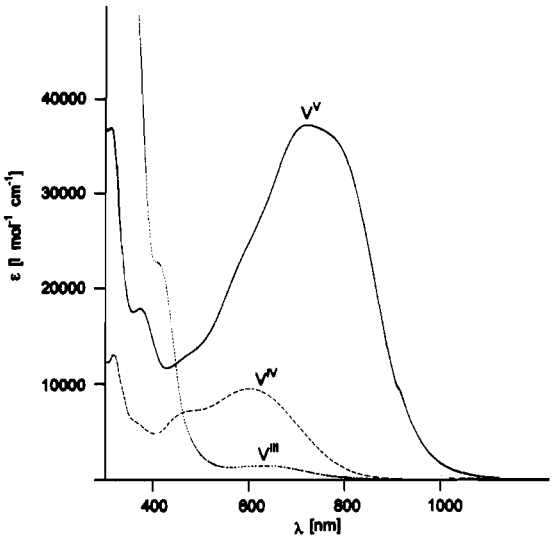

Figure 8. Electronic spectra of $[LV^{III}]$ (···), $[LV^{IV}](ClO_4)$ (- - -), and $[LV^{V}](ClO_4)_2$ (—) in CH_3CN at ambient temperature.

complex[30] (389 nm; 9.3×10^3 L mol^{-1} cm^{-1}) and the observation that yellow $[LTiCl_3]^+$ shows such a transition at 380 nm but with a much smaller molar absorption coefficient of 350 L mol^{-1} cm^{-1}.[31] On the other hand, this absorption could also have π–π^* character. It is known that substitution of phenol in the para position by an electron-donating group such as *tert*-butyl in addition to an electron-withdrawing substituent at the phenolic oxygen atom (Ti(IV)) brings about a bathochromic shift of the aromatic π–π^* transition.[32]

The spectrum of $[LV^V]^{2+}$—also a d^0 system—is interesting in this respect because the ligand-to-metal charge-transfer band is shifted to 719 nm with an extraordinary large molar absorption coefficient of 3.7×10^4 L mol^{-1} cm^{-1}. Figure 8 shows the electronic spectra of **2**–**4** all of which display a very intense low-energy transition in the visible. This absorption shifts to longer wavelengths on increasing the formal oxidation state of the vanadium ion and, concomitantly, its molar absorption coefficient increases.

It is noteworthy that species $[LM]^{n+}$ containing a metal ion with d^0, d^1, and d^2 electronic configuration display this intense charge-transfer transition in the visible. It is therefore surprising that the spectra of **5** and **6**, which contain d^3 and high-spin d^4 metal ions, respectively, do not show a CT transition in the visible. Intense d–d transitions are observed instead. Assuming, for the sake of simplicity, octahedral symmetry (O_h) for **5** the two d–d transitions observed at 569 (410) and 431 (220) nm may be assigned $^4A_{2g}(F) \rightarrow {}^4T_{2g}(F)$ and $^4A_{2g}(F) \rightarrow {}^4T_{1g}(F)$. The same assignment has been reported for $K_3[Cr(cat)_3]$ (cat = catecholate) and $(NH_4)_3[Cr(enterobactin)]$.[33] Ligand field parameters $10Dq$ of 17 570 cm^{-1} and a Racah parameter of B = 517 cm^{-1} are derived for **5**. The structurally very similar complex Cr^{III}(TCTA)[17] (TCTA = 1,4,7-triazacyclononane-1,4,7-trisacetate) which also contains a *fac*-(N_3O_3) donor set shows a very similar electronic spectrum: 388 (220), 512 (340) nm, $10Dq$ = 19 530 cm^{-1}. The data clearly indicate the absence of appreciable d_π–p_π bonding of the phenolate oxygen atoms to the chromium(III) center. Similar arguments may hold for the Mn(III) complex **6**, where one d–d transition ($^5E_g \rightarrow {}^5T_{2g}$) is observed at 629 (895) nm.

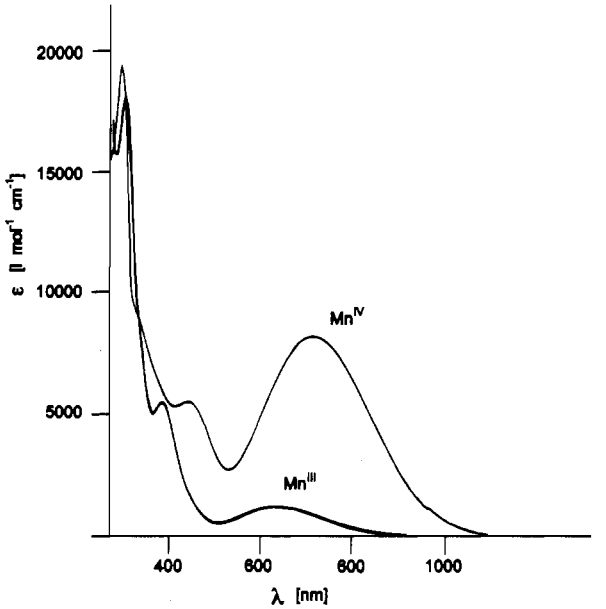

Figure 9. Electronic spectra of $[LMn^{III}]$ and $[LMn^{IV}]BPh_4$ in CH_3CN at ambient temperature.

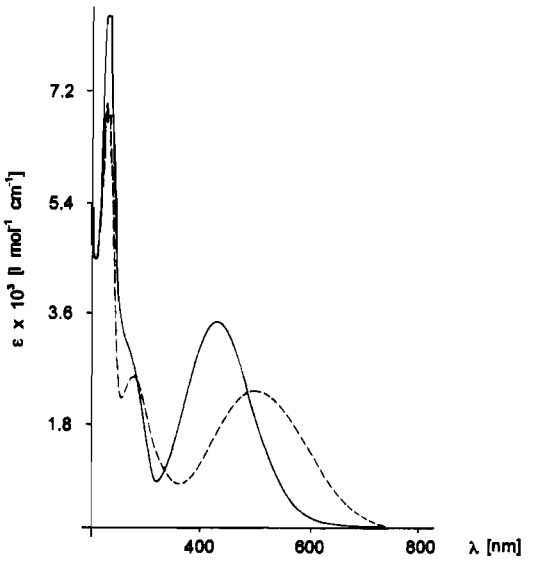

Figure 10. Electronic spectra of $[LFe^{III}]$ (—) and its protonated form (- - -) in $CH_3CN/HClO_4$ at ambient temperature.

Figure 9 shows the spectra of LMn^{III} and $[LMn^{IV}]^+$. The spectrum of $[LMn^{IV}]^+$ is interesting because Mn(IV) has a d^3 electronic configuration and its spectrum may be compared with that of **5**. Clearly, an intense CT band is observed at 640 nm contrasting in this respect the spectrum of **5**. A similar spectrum has been reported for bis(*N*-(2-carboxyethyl)salicylideneaminato)manganese(IV).[34] $[Mn^{IV}(cat)_3]^{2-}$ also displays an intense CT band in the visible at 585 nm.[35]

Electronic spectra of $[LFe^{III}]$ (**8**) and its protonated form $[(LH)_2Fe_2]^{2+}$ (**11**) are shown in Figure 10. The former exhibits a very intense CT band in the visible as do all (phenolato)iron(III) complexes.[36-38] The shoulder at 320 nm in both spectra is probably due to an amine-to-iron CT, which is practically not affected by

(30) Borgias, B. A.; Cooper, S. R.; Koh, Y. B.; Raymond, K. N. *Inorg. Chem.* **1984**, *23*, 1009.
(31) Bodner, A.; Jeske, P.; Weyhermüller, T.; Wieghardt, K.; Dubler, E.; Schmalle, H.; Nuber, B. *Inorg. Chem.* **1992**, *31*, 3737.
(32) Hesse, M.; Meier, B.; Zeeh, B. *Spectroscopic Methods in Organic Chemistry*; Georg Thieme Verlag: Stuttgart, New York, 1984.
(33) (a) Isied, S. S.; Kuo, G.; Raymond, K. N. *J. Am. Chem. Soc.* **1976**, *98*, 1763. (b) Patch, M. G.; Simolo, K. P.; Carrano, C. J. *Inorg. Chem.* **1982**, *21*, 2972.
(34) Chandra, S. K.; Basu, P.; Ray, D.; Pal, S.; Chakravorty, A. *Inorg. Chem.* **1990**, *29*, 2423.
(35) Hartman, J. R.; Foxman, B. M.; Cooper, S. R. *Inorg. Chem.* **1984**, *23*, 1381.
(36) Ackermann, G.; Hesse, D. *Z. Anorg. Allg. Chem.* **1969**, *368*, 25; **1970**, *375*, 77.
(37) Gaber, B. P.; Miskowski, V.; Spiro, T. G. *J. Am. Chem. Soc.* **1974**, *96*, 6868.
(38) Flassbeck, C.; Wieghardt, K. *Z. Anorg. Allg. Chem.* **1992**, *608*, 60.

Chart II

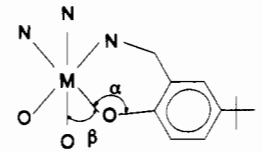

the nature of the substituted phenolate rings. This absorption has been observed in all (1,4,7-triazacyclononane)iron(III) complexes.[38] The CT band at 485 nm in **8** is shifted to longer wavelengths in the protonated form **11**.

The low-energy d–d band at 548 nm in the spectrum of **10** is shifted to a longer wavelength at 569 nm upon deprotonation to **5**. Thus the chromium(III) ion in the protonated form is in a stronger ligand field than the unprotonated form. This is somewhat counterintuitive if one considers that protonation of a phenolate oxygen atom results in a weakening of the Cr–O bond. The effect may indicate the presence of some d_π–p_π bonding, which is slightly more pronounced in **5** and is reduced by protonation in **10**. Strong π-donation of the phenolate oxygen atoms reduces the magnitude of ligand field splitting parameter $10Dq$. It is noted that the reverse behavior is observed for **9** and its protonated form **12**, where the lowest energy d–d transition is shifted from 562 nm in **9** to 660 nm in **12**. This is in accord with the expectation that no d_π–p_π bonding occurs in **9** and **12** and that weakening of a Co–O bond in **9** by protonation causes a decrease of the strength of the ligand field.

Discussion

The present series of trisphenolato metal complexes is ideally suited to study the effect of phenolato-to-metal p_π–d_π interactions as a function of the d^n electronic configuration.[39] We identify the following structural parameters which are sensitive to the actual extent of the p_π–d_π bonding of the phenolate-oxygen–metal bonds.

(i) The experimental M–O distance (Tables IV and V) may be compared with the sum of the ionic radii of the respective metal ion in an octahedral ligand environment and an O^{2-} ion, which gives an estimate for a M–O single bond. The larger the difference between these two distances, the stronger the p_π–d_π bonding (Table V). Concomitantly, the M–N_{amine} distances should reflect the degree of p_π–d_π bonding of the M–O bonds because strong M=O double bonding is expected to induce a significant structural trans influence on the M–N bond in trans position to the M–O bond.

(ii) The M–O–C and the O–M–O bond angles α and β (Chart II) are also a measure for the degree of p_π–d_π bonding. $L''WO_3{\cdot}3H_2O$[40] and $[L'''ReO_3]^+$ [41] (L'' represents 1,4,7-trimethyl-1,4,7-triazacyclononane and L''' is 1,4,7-triazacyclononane) are typical examples with a sterically unrestrained *cis*-trioxometal entity exhibiting considerable M=O double-bond character. The O–M–O angles deviate from the ideal octahedral angle of 90° (Table IV); they are obtuse. These two compounds serve as a standard for a sterically unhindered effect of strong p_π–d_π bonding on the O–M–O angle.

The M–O–C bond angle is expected to vary with the degree of p_π–d_π bonding:

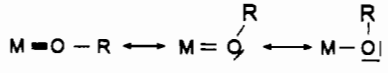

In the present series this angle α is not completely independent of the steric demands of the six-membered chelate ring M–O–C–C–C–N, but the ring size does allow some flexibility.

(iii) Finally, the phenolic O–C bond distance is expected to vary with the degree of M–O p_π–d_π bonding as may be envisaged from the following resonance structures:

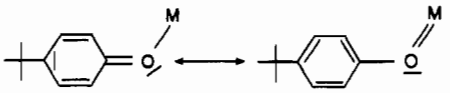

The effect on the O–C distance is experimentally not significant in the crystal structure determinations (Table IV). On the other hand, the ν(C–O) stretching frequency is readily identified in the infrared spectra of complexes. Table IX shows that this mode is shifted from 1249 cm^{-1} in **1** to 1298 cm^{-1} in **9**. These two complexes represent the two extremes as we show below; **1** displays p_π–d_π M–O bonding whereas **9** lacks this effect.

Table IX. ν(C–O) Stretching Frequency of $[LM]^{n+}$ Complexes (n = 0, 1, 2)

compd	ν(C–O), cm^{-1}	$t_{2g}^n e_g^m$ [a] n	m	c/R [b]
1	1249	0	0	6.6
2	1285	2	0	
3	1251	1	0	
4	1247	0	0	9.3
5	1294	3	0	4.8
6	1287	3	1	
7	1262	3	0	7.4
8	1290	3	2	
9	1298	6	0	

[a] Electronic configuration of the central metal ion. [b] Ratio of charge to ionic radius.

Comparison of the data in Tables IV, V, VIII, and IX reveals that complex $[LTi^{IV}]^+$ shows the most pronounced p_π–d_π bonding of the phenolate oxygen atoms: The Ti–O distances are the shortest, and they exert a pronounced structural trans influence on the Ti–N bonds. The O–Ti–O angle β is opened up and compares nicely with corresponding angles in $L''WO_3{\cdot}3H_2O$ and $[L'''ReO_3]^+$. The Ti–O–C angles are also the largest of the series, and the phenolic O–C bonds are the weakest in the series **1**–**9**. On the other extreme, complexes $[Ga(txtacn)]H^{+}$ [2] (d^0) and LCo^{III} (**9**) (d^6 low spin) (Table V) clearly show the complete absence of p_π–d_π bonding: the difference between experimental Co–O and Co–N bond distances (or Ga–O and Ga–N) and the sum of the respective ionic radii is negligible. No structural trans influence is observed; the O–M–O angles are approximately 90°, and the ν(O–C) stretching frequency of **9** is observed at the highest energy of the series.

Filling of the antibonding π^* level with one electron should not affect the expected strong p_π–d_π bonding. This is indeed observed for $[LV^{IV}]^+$ (d^1) for which all the structural indicators are very similar to those found for $[LTi^{IV}]^+$. If the π^* orbitals are further filled with two (d^2) or three (d^3) electrons, an increasing weakening of the p_π–d_π bonding should be observed, and for a low-spin d^6 electronic configuration (d_{xy}^2, d_{xz}^2, d_{yz}^2) a p_π–d_π bonding effect should not be observed. This is indeed the case for $[V^{III}(BBPEN)]^+$ [42] and $[LCr^{III}]$, where the former shows all the characteristics of relatively strong p_π–d_π bonding whereas for the latter complete absence of this effect must be concluded. It is therefore rather surprising that $[LMn^{IV}]^+$ (d^3) shows a ν(C–O) stretching frequency at 1262 cm^{-1} and a typical oxygen-to-metal CT band in the electronic spectrum. Both properties indicate the presence of p_π–d_π bonding.

(39) Nugent, W. A.; Mayer, J. M. *Metal-Ligand Multiple Bonds*; Wiley: New York, 1988; p 33.
(40) Schreiber, P.; Wieghardt, K.; Nuber, B.; Weiss, J. *Z. Anorg. Allg. Chem.* **1990**, *587*, 174.
(41) Wieghardt, K.; Pomp, C.; Nuber, B.; Weiss, J. *Inorg. Chem.* **1986**, *25*, 1659.
(42) Neves, A.; Ceccato, A. S.; Erthal, S. M. D.; Vencato, I.; Nuber, B.; Weiss, J. *Inorg. Chim. Acta* **1991**, *187*, 119.

The results for [LMn] (d^4) high spin and even more for [LFe] (d^5 high spin) are puzzling because for both species (especially the latter) p_π–d_π bonding is clearly indicated by all the available structural and spectroscopic indicators.

The most important feature of this study is the observation that the new hexadentate ligand 1,4,7-tris(5-*tert*-butyl-2-hydroxybenzyl)-1,4,7-triazacyclononane forms extremely stable pseudooctahedral complexes with tri-, tetra-, and even pentavalent first-row transition metal ions. In the presence of protons the ligand is capable of displacing terminal oxo groups in vanadyl(IV) and -(V) compounds. It was found that the fewer electrons there are in the t_{2g} valence subshell of the respective metal ion the stronger the resulting M–$O_{phenolate}$ bonds. The ligand thus stabilizes high oxidation states remarkably well. The stability of $[LM]^+$ and $[LM]^{2+}$ species **1**, **3**, **4**, and **7** in solution over the pH range 0–14 is also quite remarkable. No dissociation of the ligand or protonation at the phenolate oxygen is observed. In contrast, the neutral species [LM] (**5**), **8**, and **9** are protonated in acidic solution and formation of dimeric species $[(LH)_2M_2]^{2+}$ is observed, but here also no ligand dissociation occurs. In alkaline solution these complexes are also very stable. In particular, no precipitation of $Fe(OH)_3$ from alkaline solutions of **8** has been observed. In a subsequent paper we will show that the residual basicity of the coordinated phenolate oxygen atoms in **5**, **8**, and **9** can be exploited. These complexes may be used as ligands, and the synthesis of trinuclear species $[LCo^{III}M^{II}Co^{III}L]^{2+}$ and $[LFe^{III}(H_2O)_3M(H_2O)_3Fe^{III}L]^{2+}$ ($M = Mn^{II}, Co^{II}, Ni^{II}, Zn^{II}$) will be described.

Acknowledgment. We thank the Fonds der Chemischen Industrie for financial support of this work.

Supplementary Material Available: For the crystallographically characterized complexes **1**, **5**, **8**, and **11**, tables listing details of data collection, structure solution, and refinement, bond distances and angles, anisotropic thermal parameters, and positional parameters of the hydrogen atoms (calculated) and, for **5** and **8**, figures showing perspective views and atom-labeling schemes (30 pages). Ordering information is given on any current masthead page.